

Topological Engineering of High-Order Exceptional Points through Transformation Optics

Kaiyuan Wang ^{1,2}, Qi Jie Wang ^{1,3}, Matthew R. Foreman ^{1,2,*} and Yu Luo ^{4,†}

¹*School of Electrical and Electronic Engineering,*

Nanyang Technological University, 50 Nanyang Avenue, Singapore 639798

²*Institute for Digital Molecular Analytics and Science, 59 Nanyang Drive, Singapore 636921*

³*Centre for Disruptive Photonic Technologies, School of Physical and Mathematical Sciences, Nanyang Technological University, Singapore, Singapore*

⁴*National Key Laboratory of Microwave Photonics,*

Nanjing University of Aeronautics and Astronautics, Nanjing 211106, China

(Dated: March 18, 2025)

Exceptional points (EPs) in non-Hermitian photonic systems have attracted considerable research interest due to their singular eigenvalue topology and associated anomalous physical phenomena. These properties enable diverse applications ranging from enhanced quantum metrology to chiral light-matter interactions. Practical implementation of high order EPs in optical platforms however remains fundamentally challenging, requiring precise multi-parameter control that often exceeds conventional design capabilities. This work presents a novel framework for engineering high order EPs through transformation optics (TO) principles, establishing a direct correspondence between mathematical singularities and physically controllable parameters. Our TO-based paradigm addresses critical limitations in conventional Hamiltonian approaches, where abstract parameter spaces lack explicit connections to experimentally accessible degrees of freedom, while simultaneously providing full-field mode solutions. In contrast to prevailing parity-time-symmetric architectures, our methodology eliminates symmetry constraints in EP design, significantly expanding the possibilities in non-Hermitian photonic engineering. The proposed technique enables unprecedented control over EP formation and evolution in nanophotonic systems, offering new pathways for developing topological optical devices with enhanced functionality and robustness.

I. INTRODUCTION

An exceptional point (EP) is a branch point singularity that can occur in the spectrum of non-Hermitian systems. An N -th order EP (denoted henceforth as EP N) corresponds to a point in the system's parameter space at which N eigenvalues and the associated eigenstates of the non-Hermitian Hamiltonian coalesce [1, 2]. EPs have been extensively studied in recent years as they can give rise to unique physical phenomena, such as unidirectional invisibility [3, 4], enhanced sensitivity [5, 6], and non-reciprocal light propagation [7]. Advances in this field have also revealed a variety of complex EP geometries in parameter space, including exceptional rings [8, 9], arcs [10, 11], surfaces [12], and junctions [13], which can exhibit diverse features like fractional topological charges [14, 15] and an anisotropic response to external perturbations [16, 17]. These properties offer significant opportunities to tailor the response of physical systems.

Nano- and micro-optical systems, including microcavities, waveguides, gratings, and nanoplasmonic structures [18, 19], have proven to be rich and flexible platforms for realizing, studying, and engineering EPs. For example, the observation of EPs in microcavity systems has enabled enhanced optical sensing capabilities [5, 20], while EPs in waveguides have facilitated the development

of novel light manipulation techniques [21, 22]. Current methods to design EPs in optical systems however primarily focus on the system Hamiltonian. Whilst effective in theoretical studies, the Hamiltonian approach faces significant challenges when applied to EP design in realistic physical systems. For instance, Hamiltonians considered in EP design are often limited to idealised or simplified models which do not accurately represent the complexity or capture intricate interactions present in practical systems, especially at the nanoscale. Such issues are further compounded in the design of high order exceptional points, which requires precise adjustment of $2N - 2$ real parameters in general, which is challenging in practice [22, 23]. Although specific symmetries, such as pseudo-Hermitian, or chiral symmetry, can help reduce the difficulty of finding EPs [24, 25], generalizing these symmetries to the generation of higher-order EPs remains an open problem [26, 27].

In this work, we propose an approach to design high order EPs which leverages transformation optics (TO) and is capable of alleviating limitations of the Hamiltonian based approach. TO is a powerful and versatile method that allows manipulation of electromagnetic fields through engineering material properties [28]. The flexibility of TO allows us to not only model complex geometries but also to design EPs with specific mode distributions. Our approach moreover does not rely on PT symmetry, thereby enabling the design of non-PT symmetric EPs, which have garnered significant attention due to their broader range of unique properties [19, 29–

* matthew.foreman@ntu.edu.sg

† yu.luo@nuaa.edu.cn

31].

II. DESIGN PRINCIPLES AND RESULTS

Transformation optics exploits the invariance of Maxwell's equations under coordinate transformations, such that known electromagnetic solutions for simple geometries can be mapped to more complex structures [32, 33]. By first deriving the canonical resonance condition for modes in a planar multilayered structure, we can conveniently tailor the physical parameters of the system to generate high order EPs, before the solution is finally mapped to a more complicated geometry. In this work we focus on design of EPs in nanoplasmonic systems. Noting that in a multilayer geometry, each interface can potentially support a surface plasmon polariton (SPP) mode, an N th order EP can thus in principle be designed for a system with N interfaces ($N + 1$ layers) [22]. Existence of an N th order EP, however, requires that the resonance equation be expressible as an N th order polynomial in one of the frequency dependent system parameters (typically electric permittivity), and that this polynomial possesses N repeated roots. These constraints help guide system design and allow us to determine suitable material and geometric parameters to realise high order EPs.

For concreteness, we illustrate the approach through construction and analysis of a third-order EP in a coupled core-shell/monomer nanowire system as depicted in Figure 1(a). We therefore begin by considering a general two-dimensional four layer system, with electric permittivities ϵ_j for integer $j \in [1, 4]$ and interface separations d_1 and d_2 as shown in Figure 1(a). In the quasi-static limit, we can express supported modes in terms of their scalar potential distribution, from which we can derive the corresponding electric and displacement fields, \mathbf{E} and \mathbf{D} respectively (see the Supplementary Material for further details and alternative derivations). Application of standard boundary conditions for the tangential (normal) components of the electric (displacement) field at each interface yields a set of linear equations relating the tangential electric field component at each interface, specifically

$$\mathbb{M}^{(3)}\mathbf{E}^{(3)} = \mathbf{0} \quad (1)$$

where

$$\mathbb{M}^{(3)} = \begin{bmatrix} \mathcal{M}(d_2, \epsilon_2, \epsilon_1) & -\epsilon_2 & 0 \\ 0 & -\epsilon_3 & \mathcal{M}(d_1, \epsilon_3, \epsilon_4) \\ \mathcal{M}(d_2, \epsilon_1, \epsilon_2) & 0 & \mathcal{M}(d_1, \epsilon_4, \epsilon_3) \end{bmatrix}, \quad (2)$$

$$\mathbf{E}^{(3)} = \begin{bmatrix} E_y(x_0 - d_2) \\ E_y(x_0) \\ E_y(x_0 + d_1) \end{bmatrix}, \quad (3)$$

$\mathcal{M}(d, \epsilon_a, \epsilon_b) = \epsilon_a \cosh(|k|d) + \epsilon_b \sinh(|k|d)$ and k is the free space wavenumber. Resonances correspond to non-trivial

solutions of Eq. (S30) which occur when

$$\det[\mathbb{M}^{(3)}] = \epsilon_2 \mathcal{M}(d_1, \epsilon_3, \epsilon_4) \mathcal{M}(d_2, \epsilon_1, \epsilon_2) + \epsilon_3 \mathcal{M}(d_1, \epsilon_4, \epsilon_3) \mathcal{M}(d_2, \epsilon_2, \epsilon_2) = 0. \quad (4)$$

Eq. (S32) in its most general form is quadratic in the permittivity of any given layer and therefore it is not readily apparent how to design EPs of order higher than 2. By asserting, however, that two layers have identical permittivity (whilst keeping the number of interfaces fixed), Eq. (S32) can be expressed as a cubic equation. Specifically, if we assume $\epsilon_1 = \epsilon_3 = \epsilon_m$ (which we take as a lossy metal in what follows), $\epsilon_2 = \epsilon_h$ (a 'host' dielectric material) and $\epsilon_4 = \epsilon_d$ (dielectric), Eq. (S32) can be written as

$$A\epsilon_m^3 + B\epsilon_m^2 + C\epsilon_m + D = 0, \quad (5)$$

where the coefficients are defined in the Supplementary Material. Notably, these material choices do not correspond to a PT symmetric system. Furthermore, note that Eq. (S47) can be considered as the characteristic equation of some eigenvalue problem $|\mathbb{A} - \epsilon_m \mathbb{I}| = 0$, such that we will refer to values of ϵ_m satisfying Eq. (S47) (denoted $\epsilon_{m,r}$ for $r = 1, 2, 3$) as eigenvalues. The corresponding frequencies ω_r for which $\epsilon_m(\omega_r) = \epsilon_{m,r}$ shall be termed resonant eigenfrequencies. To generate a third order degeneracy we apply the well known criteria for a cubic equation to have three repeated roots. Specifically, letting the discriminant $\Delta = (4\Delta_1^3 - \Delta_2^2)/(27A^2)$, where $\Delta_1 = B^2 - 3AC$ and $\Delta_2 = 2B^3 - 9ABC + 27A^2D$ [34], we require $\Delta = \Delta_1 = 0$. For our example, the repeated root is then given by

$$\epsilon_m = -\frac{B}{3A} = -\frac{1}{3}(\epsilon_h[1 + \coth(kd_1)] \coth(kd_2) + \epsilon_d \coth(kd_1)). \quad (6)$$

Noting that the metal is lossy and that k , d_1 and d_2 are real positive numbers, Eq. (6) implies that either ϵ_h or ϵ_d (or both) must have an imaginary part of opposite sign to ϵ_m , i.e. must possess gain. Henceforth, we consider the case $\text{Im}[\epsilon_h] = 0$ and that ϵ_d describes a material with gain, as depicted in Figure 1(a). According to the principles of TO, the same conditions also govern the mode spectrum in the coupled nanowire geometry shown on the right of Figure 1(a), which can be generated through application of the exponential conformal mapping [35]:

$$w' = \frac{g}{\exp(w) - 1} \quad (7)$$

where $w^{(i)} = x^{(i)} + iy^{(i)}$, (x, y) are the untransformed spatial coordinates and primes denote transformed quantities. The parameter g is a scaling constant that controls the diameter of the nanowires (D_1, D_2, D_3 defined in the Supplement) in the transformed geometry. We assume that g is chosen such that the dimensions of the nanowire system are smaller than the optical wavelength,

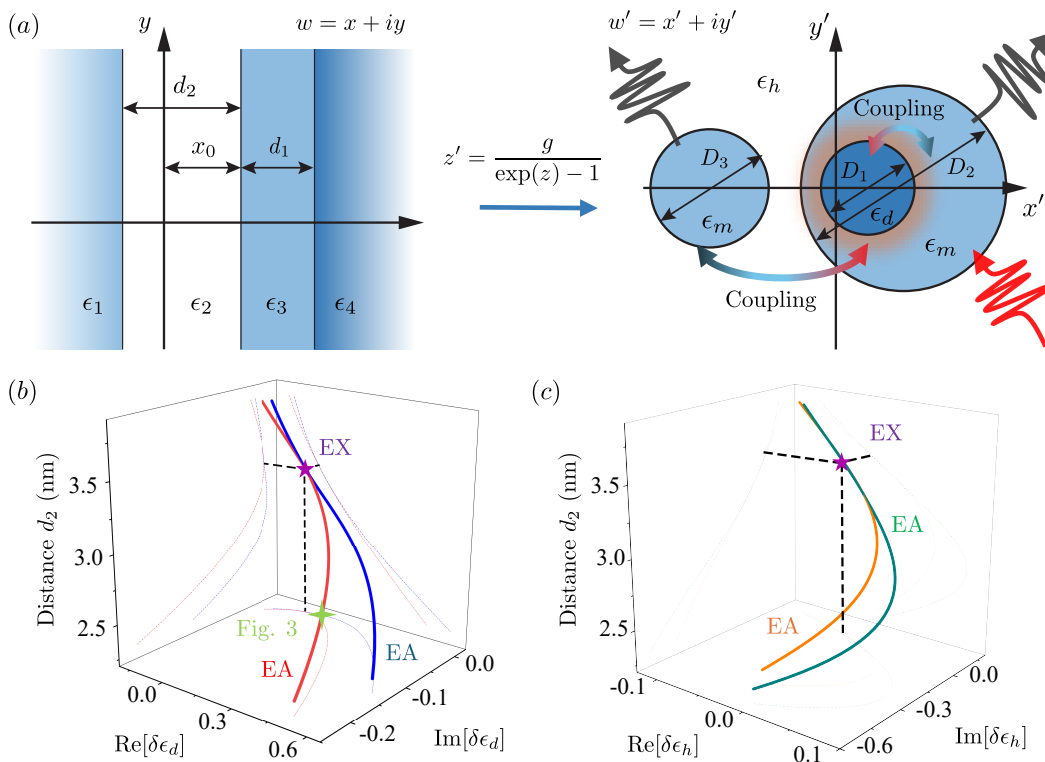


FIG. 1. **TO approach to designing exceptional points.** (a) Schematic diagram of planar geometry considered before (left) and plasmonic nanowire geometry consider after (right) transformation. (b) Exceptional arcs and nexus traced in physical parameter space upon variation of electric permittivity of gain material and interface separation d_2 . (c) As (b) albeit for variations in host material.

whereby the quasi-static model holds. Within this limit, the change in permeability after transformation can also be ignored [36]. Finally, we note, that the periodicity of the transformation implies $k = n$ ($n \in \mathbb{Z}$), which physically corresponds to the angular momentum of the corresponding mode.

For material and geometric parameters satisfying $\Delta = \Delta_1 = 0$ and Eq. (6), the solutions of Eq. (S32) are threefold degenerate. Accordingly, these equations describe necessary parametric constraints which must be fulfilled to realise an EP3 and hence provides direct physical insight into the design of high order EPs. For example, assuming a fixed host material (here taken as water with $\epsilon_h = 1.76$), and interface separation d_1 the constraints $\Delta = \Delta_1 = 0$ allow us to select appropriate dielectric materials (and corresponding required levels of gain) and nanowire radii, such that Eq. (6) dictates the necessary metal permittivity to generate a third order degenerate point. Using known metallic dispersion equations (taken here as the Drude-Sommerfeld model with $\epsilon_\infty = 5$, $\omega_p = 8.9$ eV, $\Gamma = 18$ fs corresponding to silver [37]), the degenerate eigenfrequency can then be found. Assuming, $d_1 = 0.84$, $x_0 = 0.1$ and $m = 1$, we find from the repeated root constraints that $d_2 = 2$ (yielding $D_1 = 199$ nm, $D_2 = 18$ nm and

$D_3 = 6$ nm for $g = 2 \times 10^{-8}$). Eq. (6) then yields $\epsilon_m = (-1.548 + 0.856i)$ corresponding to a third order degeneracy at $\omega_{EP} = (8.352 + 0.250i) \times 10^{14}$ Hz. We neglect non-local effects in the material permittivities for simplicity [38, 39].

To verify the degeneracy of the modes predicted using the TO approach and its exceptional nature, we analyze the properties of the nanowire system in the vicinity of the expected EP3. In Figure 2(a) we present a plot of the logarithm of the scattering cross-section calculated as a function of gain and frequency using the method described in Ref. [40]. Selected line profiles (denoted I–V) are also shown in Figure 2(b), in which evolution of individual spectral peaks with material gain is illustrated. At low gains (line profile I and II), three spectral peaks are evident, which merge into a single broad peak at the EP3 (line profile III) before splitting again as gain is increased further (line profile IV and V). Accompanying blue data markers in Figure 2(b), found via rigorous finite element COMSOL simulations, indicate good agreement with the theoretical TO based calculations. Solid coloured lines in Figure 2(a) represent the real part of the eigenfrequencies, i.e. $\text{Re}[\omega_r]$, calculated via numerical solution of Eq. (S47). In general three distinct modes are found, however at the predicted EP the real part of the

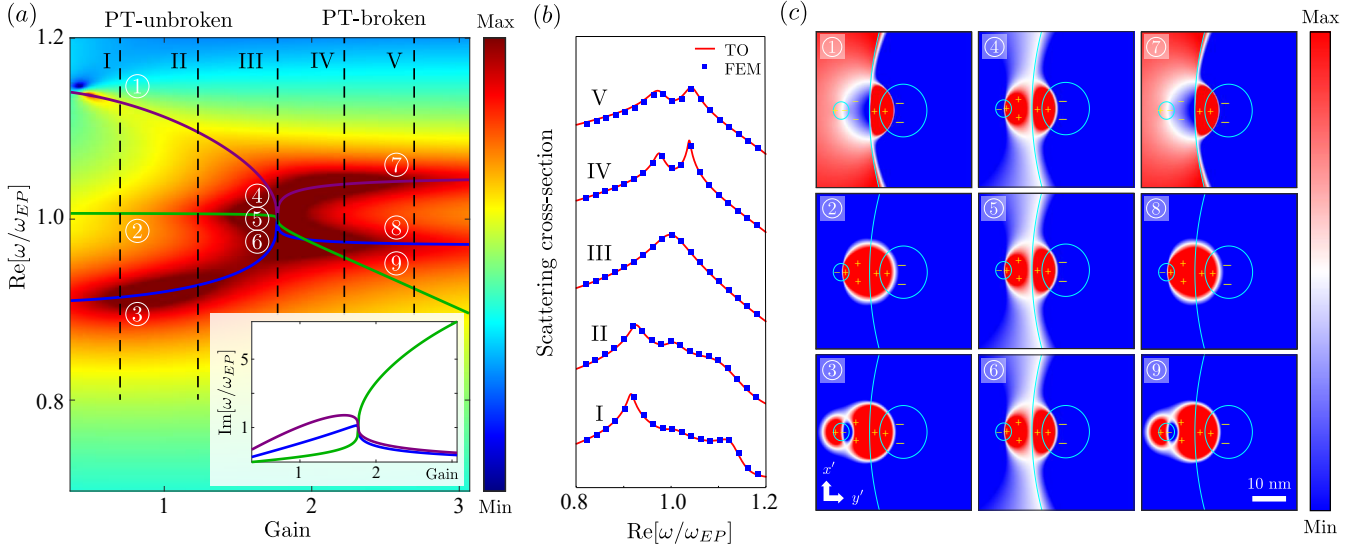


FIG. 2. **EP3 in core-shell/monomer coupled nanowire system.** (a) Color density plot of the logarithm of the scattering cross-section of the coupled core-shell and monomer structures as a function of gain and frequency. Solid lines represent the real parts of the three eigenfrequencies (corresponding imaginary parts are shown in the inset). (b) scattering cross-sections corresponding to I-V in (a) as found using our TO approach (red lines) and finite element simulations (blue markers). (c) Potential distributions for eigenmodes at points labelled ①–⑨ in (a). Cyan lines demark the nanowire interfaces (only a small part of core-shell nanowire in vicinity of monomer is shown to enhance visibility). Panels ④–⑥ correspond to the EP3.

eigenfrequencies clearly coalesce. The inset in the lower right of Figure 2(a) shows the corresponding coalescence of the imaginary part of the eigenfrequency and illustrates the significant changes in loss associated with the emergence of the EP [41]. Specifically, in the PT-like unbroken phase, the mode corresponding to the green line exhibits relatively low loss, whereas in the PT-like broken phase, the loss increases sharply resulting in relatively weak scattering. In contrast, the loss for the other modes (blue and purple lines), decreases with increasing gain in the PT-like broken phase. This strong difference in loss means that at higher gains, only the two low loss spectral peaks are visible in the scattering spectrum (line profiles IV and V).

Degeneracy in the complex eigenfrequencies, whilst suggestive, does not unequivocally demonstrate that solutions to Eq. (S47) correspond to an EP. To demonstrate that the found degenerate point is indeed an EP3, we also show that the mode distributions for each eigenfrequency are identical at the degenerate point. Our TO method can fortunately provide direct information about the potential distributions for each plasmonic mode, which is often beyond the reach of traditional Hamiltonian approaches without additional modelling. Specifically, through Gaussian elimination it is simple to show that the solutions to Eq. (S30) take the form (with our mate-

rial assumptions)

$$\begin{bmatrix} E_y(x_0 - d_2) \\ E_y(x_0) \\ E_y(x_0 + d_1) \end{bmatrix} = \begin{bmatrix} 1 \\ \epsilon_h^{-1} \mathcal{M}(d_2, \epsilon_h, \epsilon_m) \\ \frac{\epsilon_m \mathcal{M}(d_2, \epsilon_h, \epsilon_m)}{\epsilon_h \mathcal{M}(d_2, \epsilon_m, \epsilon_d)} \end{bmatrix}, \quad (8)$$

from which the full potential distributions follow. Example distributions are shown in Figure 2(c) for the points ①–⑨ on the resonance branches indicated in Figure 2(a). Color scales for each diagram span the respective maximum and minimum potential and are not necessarily the same for each panel. For non-degenerate conditions (①–③) and (⑦–⑨) the nanowire structure exhibits standard plasmonic modes, including symmetric and asymmetric distributions at different boundaries. In contrast, at the degenerate point, the modes found for each branch are identical (④–⑥) as expected for an EP. Moreover, the distributions are highly confined and exhibit unique spatial distributions not observed in lower order EPs. These patterns thus highlight the complexity and richness of the physical phenomena occurring at higher-order EPs.

Relaxing our previous constraint that $\Delta_1 = 0$, whilst still requiring that the discriminant of Eq. (S47) be zero ($\Delta = 0$), implies that Eq. (S47) possesses only two repeated roots [34]. We find that $\Delta = 0$ therefore defines curves in parameter space corresponding to systems supporting second (lower) order EPs. To illustrate this point we introduce perturbations $\delta\epsilon_h$ and $\delta\epsilon_d$, corresponding to variations in the complex electric permittivity of the host and dielectric gain material respectively, away from the EP3. Figure 1(b) shows the resulting EP2 exceptional

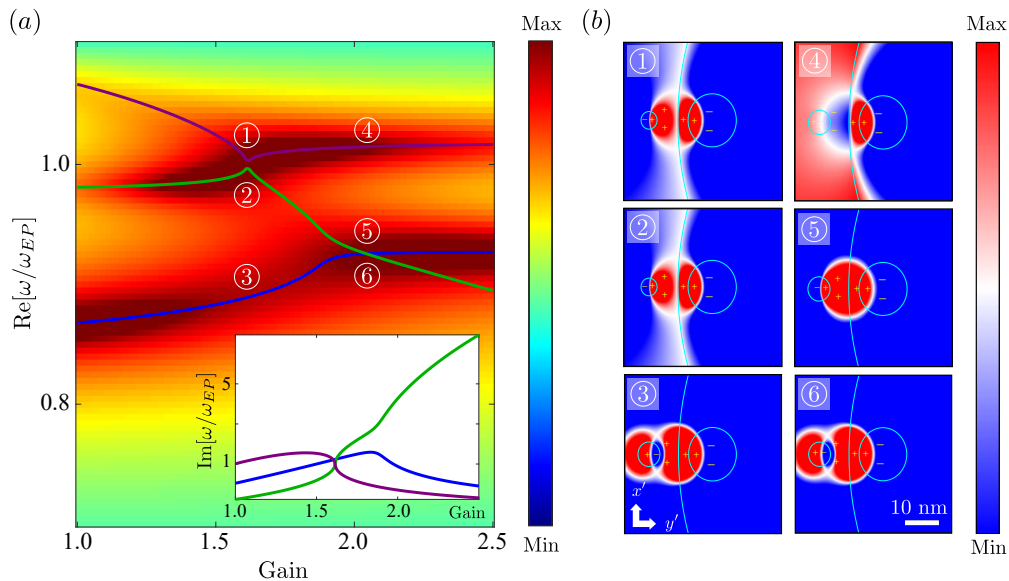


FIG. 3. **EP2 in core-shell/monomer coupled nanowire system** (a) As Figure 2(a) albeit for system parameters lying on the EA away from the EX (see Figure 1) (b) Potential distributions for ①-⑥ in (a). Panels ① and ② correspond to the crossing of the real part of the eigenfrequencies, whereas the identical distributions in ⑤ and ⑥ signify an EP2.

arcs (EA) [10, 11] in the $(d_2, \delta\epsilon_h)$ domain when $\delta\epsilon_d = 0$. Similarly, Figure 1(c) illustrates the case for perturbations in the gain material ($\delta\epsilon_d \neq 0, \delta\epsilon_h = 0$). Note that in each case two arcs result since Δ is quadratic in the corresponding system parameters. Through our TO analysis we can therefore easily determine the family of coupled nanowire configurations supporting EP2s, and how to tune particular parameters (such as wire radius) to move along these EAs to reach the point of convergence, i.e. the exceptional nexus (EX), and generate the resulting higher order EP3. We note that this insight and practical tunability is typically absent from Hermitian based design philosophies which consider more abstracted perturbations, e.g., to modal coupling constants, in contrast to the real physically relevant perturbations considered in our model. Figure 3(a) analyzes the EP2 at a position along the exceptional EA (beyond the range of parameter variation shown in Figure 1), in a manner similar to Figure 2. We first note that, as shown in Figure 3(a), the eigenfrequencies corresponding to the purple and green solid lines possess the same real and imaginary parts for gains ~ 1.6 , indicating the presence of an EP2, which is confirmed by the degenerate mode distributions shown in panels ⑤ and ⑥ of Figure 3(b). It is interesting, to note that at a gain of ~ 2 , the real parts of the eigenfrequencies traced by the blue and green curves are equal, however their imaginary parts (inset of Figure 3(a)) remain different demonstrating this point is not a true degeneracy [42].

To further demonstrate the capabilities and versatility of our method in designing higher-order EPs, we have explored two further scenerios. Firstly, we consider de-

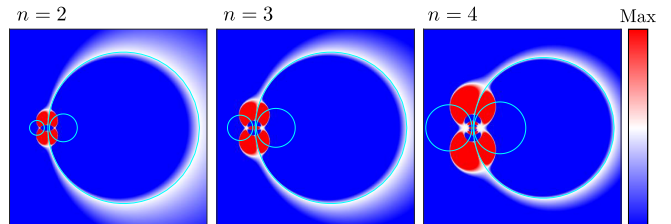


FIG. 4. **EP3s with different angular momenta.** Potential distributions for modes with angular momenta (left) $n = 2$, (middle) $n = 3$ and (right) $n = 4$, evaluated at an EP3 in a system analogous to that shown in Figure 2.

sign of EPs with different angular momenta, n . The corresponding potential distributions found for third order EPs in a core-shell/monomer nanowire system with angular momenta of $n = 2$, $n = 3$ and $n = 4$ are shown in Figure 4.

Secondly, we consider design of a fourth-order exceptional point (EP4). Specifically, by considering a 5 layer gain-loss multilayer structure distributed symmetrically around the y -axis, we can generate, through application of Eq. (7), a PT symmetric configuration of two adjacent core-shell structured nanowires. The metallic outer shell of one nanowire is assumed to be described by electric permittivity $\epsilon_m = \epsilon_\infty - \omega_p^2/\omega^2 + i\alpha$, whereas the inner dielectric core has $\epsilon_d = \epsilon - i\beta$, where α and β are frequency independent parameters, $\epsilon = 1.84$, $\epsilon_\infty = 5$ and $\omega_p = 8.9$ eV. PT symmetry therefore implies for the other nanowire the core and shell have permittivi-

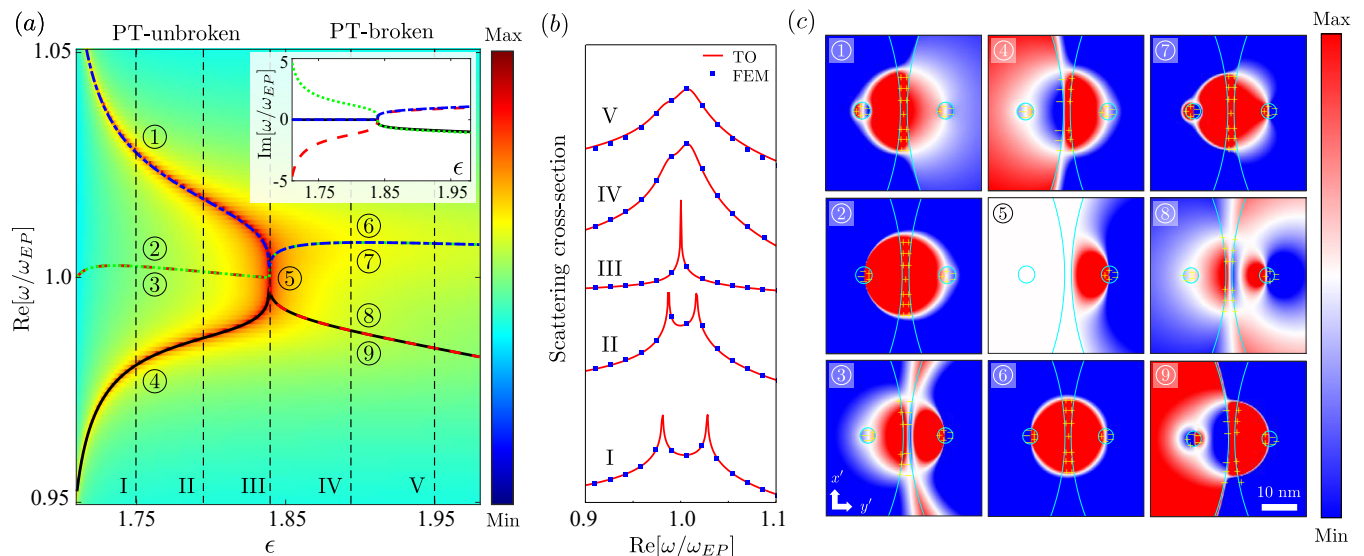


FIG. 5. **EP4 in core-shell dimer nanowire system.** (a) Color density plot of the logarithm of the scattering cross-section of the coupled core-shell dimer structure as a function of ϵ and frequency. Solid and dashed lines represent the real parts of the four eigenfrequencies (corresponding imaginary parts are shown in the inset). (b) Scattering cross-sections corresponding to I-V in (a) as found using our TO approach (red lines) and finite element simulations (blue markers). (c) Potential distributions for eigenmodes at points labelled ①-⑨ in (a). Cyan lines demark the nanowire interfaces (only a small part of core-shell nanowires are shown to enhance visibility). Panel ⑤ corresponds to the EP3.

ties ϵ_m^* and ϵ_d^* respectively. The host material is taken to be air with unity permittivity. Figure 5(a) shows the resulting distribution of the logarithmic scattering cross-section as a function of ϵ and frequency. Using the assumed analytic forms of the permittivity functions, the resonance condition can be expressed as a polynomial in frequency ω , specifically, $A\omega^8 + B\omega^6 + C\omega^4 + D\omega^2 + E = 0$, which is quartic in ω^2 with three distinct roots. As before, the curves in Figure 5(a) represent the real part of the eigenfrequencies, $\text{Re}[\omega_r]$, found from the corresponding resonance condition (see Supplementary Material). To aid visibility of overlapping branches, some curves are plotted using a dashed line style. The inset to Figure 5(a) shows the corresponding imaginary part of the eigenfrequencies as a function of relative permittivity, which exhibit significantly different behaviour between the PT-unbroken and broken phases. Symmetry in the core-shell structures also leads to the existence of dark modes, resulting in weak scattering (and low scattering cross-sections) in spite of small modal losses [43, 44]. The mode distributions can again be found (see Supplementary Material) and are shown at assorted positions along the resonance branches in Figure 5(c) as marked ①-⑨ in Figure 5(a). Constraints for the existence of multiple repeated roots (2, 3, or 4) are known [34] and can therefore be used to design exceptional points of higher order. In our case we seek an EP4 and use the constraints $8AC - 3B^2 = B^3 - 4ABC + 8A^2D = 16AB^2C - 64A^2BD - 3B^4 + 256A^3E = 0$, which yields an EP4 at position ⑤ in parameter space. The good agree-

ment between TO based predictions and rigorous COMSOL simulation results for both the scattering cross-section and mode distributions, shown in Figure 5, validates our approach.

III. CONCLUSION

This work has introduced a novel TO based approach for designing high-order EPs in nanoplasmonic systems. By utilising TO, we have mapped solutions from simple multilayer geometries to complex nanowire structures, enabling the design of EPs with targeted properties. Specifically, we have demonstrated the realization of an EP3 in a coupled core-shell/monomer nanowire system, identifying the precise constraints on system parameters required to achieve the desired degeneracy. Finite element simulations were used to confirm the existence and exceptional nature of the EP3. Furthermore, we have shown how this approach can be extended to design EP2s along exceptional arcs, revealing a pathway to higher-order EPs through parameter space manipulation. The versatility of our method was further highlighted by the demonstration of EP3s with varying angular momenta and the design of a EP4 in a coupled core-shell dimer system. Our TO-based methodology overcomes limitations of traditional Hamiltonian approaches, which often struggle to connect abstract model parameters to experimentally controllable variables. Moreover, our approach naturally yields corresponding mode distributions

without requiring additional modelling. Accordingly, the TO methodology offers a powerful and flexible framework for engineering EPs in complex nanophotonic structures, opening new avenues for applications in sensing, light manipulation, and other areas where precise control over light-matter interaction is crucial.

ACKNOWLEDGMENTS

K.W. is funded by an Interdisciplinary Graduate Programme PhD Research Scholarship through the Institute for Digital Molecular Analytics and Science (IDMxS) under the Singapore Ministry of Education Research Centres of Excellence scheme. MRF acknowledges further funding from Singapore Ministry of Education Academic Research Fund (Tier 1) Grant No. RS13/23.

-
- [1] Miri, M.-A., and Alù, A. "Exceptional points in optics and photonics." *Science* 363.6422 (2019): eaar7709. DOI: [10.1126/science.aar7709](https://doi.org/10.1126/science.aar7709)
- [2] Heiss, W. D. "The physics of exceptional points." *Journal of Physics A: Mathematical and Theoretical* 45.44 (2012): 444016. DOI: [10.1088/1751-8113/45/44/444016](https://doi.org/10.1088/1751-8113/45/44/444016)
- [3] Feng, L., Wong, Z. J., Ma, R.-M., Wang, Y., and Zhang, X. "Single-mode laser by parity-time symmetry breaking." *Science* 346.6212 (2013): 972-975. DOI: [10.1126/science.1258479](https://doi.org/10.1126/science.1258479)
- [4] Regensburger, A., Bersch, C., Miri, M.-A., Onishchukov, G., Christodoulides, D. N., and Peschel, U. "Parity-time synthetic photonic lattices." *Nature* 488.7410 (2012): 167-171. DOI: [10.1038/nature11298](https://doi.org/10.1038/nature11298)
- [5] Chen, W., Özdemir, Ş. K., Zhao, G., Wiersig, J., and Yang, L. "Exceptional points enhance sensing in an optical microcavity." *Nature* 548.7666 (2017): 192-196. DOI: [10.1038/nature23281](https://doi.org/10.1038/nature23281)
- [6] Loughlin, H., Sudhir, V. "Exceptional-point sensors offer no fundamental signal-to-noise ratio enhancement." *Physical Review Letters* 132.24 (2024): 243601. DOI: [10.1103/PhysRevLett.132.243601](https://doi.org/10.1103/PhysRevLett.132.243601)
- [7] Peng, B., Özdemir, Ş. K., Lei, F., et al. "Parity-time-symmetric whispering-gallery microcavities." *Nature Physics* 10.5 (2014): 394-398. DOI: [10.1038/nphys2927](https://doi.org/10.1038/nphys2927)
- [8] Zhen, B., Hsu, C. W., Igarashi, Y., Lu, L., Kaminer, I., Pick, A., Chua, S.-L., Joannopoulos, J. D., and Soljačić, M. "Spawning rings of exceptional points out of Dirac cones." *Nature* 525.7569 (2015): 354-358. DOI: [10.1038/nature14889](https://doi.org/10.1038/nature14889)
- [9] Cerjan, A., Huang, S., Chen, K. P., Chong, Y. D., and Rechtsman, M. C. "Experimental realization of a Weyl exceptional ring." *Nature Photonics* 13.9 (2019): 623-628. DOI: [10.1038/s41566-019-0453-z](https://doi.org/10.1038/s41566-019-0453-z)
- [10] Shen, H., Zhen, B., and Fu, L. "Topological band theory for non-Hermitian Hamiltonians." *Physical Review Letters* 120.14 (2018): 146402. DOI: [10.1103/PhysRevLett.120.146402](https://doi.org/10.1103/PhysRevLett.120.146402)
- [11] Zhou, H., Peng, C., Yoon, Y., Hsu, C. W., Nelson, K. A., Fu, L., Joannopoulos, J. D., Soljačić, M., and Zhen, B. "Observation of bulk Fermi arc and polarization half charge from paired exceptional points." *Science* 359.6379 (2018): 1009-1012. DOI: [10.1126/science.aap9859](https://doi.org/10.1126/science.aap9859)
- [12] Zhong, Q., Ren, J., Khajavikhan, M., Christodoulides, D. N., and El-Ganainy, R. "Sensing with exceptional surfaces in order to combine sensitivity with robustness." *Physical Review Letters* 122.15 (2019): 153902. DOI: [10.1103/PhysRevLett.122.153902](https://doi.org/10.1103/PhysRevLett.122.153902)
- [13] Bergholtz, E. J., and Budich, J. C. "Non-Hermitian Weyl physics in topological insulator ferromagnet junctions." *Physical Review Research* 1.1 (2019): 012003. DOI: [10.1103/PhysRevResearch.1.012003](https://doi.org/10.1103/PhysRevResearch.1.012003)
- [14] Song, F., Yao, S., and Wang, Z. "Non-Hermitian skin effect and chiral damping in open quantum systems." *Physical Review Letters* 123.17 (2019): 170401. DOI: [10.1103/PhysRevLett.123.170401](https://doi.org/10.1103/PhysRevLett.123.170401)
- [15] Cerjan, A., Xiao, M., Yuan, L., and Fan, S. "Effects of non-Hermitian perturbations on Weyl Hamiltonians with arbitrary topological charges." *Physical Review B* 97.7 (2018): 075128. DOI: [10.1103/PhysRevB.97.075128](https://doi.org/10.1103/PhysRevB.97.075128)
- [16] Pan, L., Chen, S., and Cui, X. "High-order exceptional points in ultracold Bose gases." *Physical Review A* 99.1 (2019): 011601. DOI: [10.1103/PhysRevA.99.011601](https://doi.org/10.1103/PhysRevA.99.011601)
- [17] Bergholtz, E. J., Budich, J. C., and Kunst, F. K. "Exceptional topology of non-Hermitian systems." *Reviews of Modern Physics* 93.1 (2021): 015005. DOI: [10.1103/RevModPhys.93.015005](https://doi.org/10.1103/RevModPhys.93.015005)
- [18] Yang, Z., and Zhang, B. "Non-Hermitian light control in nanophotonics." *Advanced Optical Materials* 8.10 (2020): 1901533. DOI: [10.1002/adom.201901533](https://doi.org/10.1002/adom.201901533)
- [19] Ganainy, R. E., Makris, K. G., Khajavikhan, M., Musslimani, Z. H., Rotter, S., and Christodoulides, D. N. "Non-Hermitian physics and PT symmetry." *Nature Physics* 14.1 (2018): 11-19. DOI: [10.1038/nphys4323](https://doi.org/10.1038/nphys4323)
- [20] Hodaie, H., Hassan, A. U., Wittek, S., Garcia-Gracia, H., El-Ganainy, R., Christodoulides, D. N., and Khajavikhan, M. "Enhanced sensitivity at higher-order exceptional points." *Nature* 548.7666 (2017): 187-191. DOI: [10.1038/nature23280](https://doi.org/10.1038/nature23280)
- [21] Doppler, J., Mailybaev, A. A., Böhm, J., Kuhl, U., Girschik, A., Libisch, F., Milburn, T. J., Rabl, P., Moiseyev, N., and Rotter, S. "Dynamically encircling an exceptional point for asymmetric mode switching." *Nature* 537.7618 (2016): 76-79. DOI: [10.1038/nature18605](https://doi.org/10.1038/nature18605)
- [22] Mandal, I., and Bergholtz, E. J. "Symmetry and higher-order exceptional points." *Physical Review Letters* 127.18 (2021): 186601. DOI: [10.1103/PhysRevLett.127.186601](https://doi.org/10.1103/PhysRevLett.127.186601)
- [23] Ding, K., Fang, C., and Ma, G. "Non-Hermitian topology and exceptional-point geometries." *Nature Reviews Physics* 4.12 (2022): 745-760. DOI: [10.1038/s42254-022-00491-0](https://doi.org/10.1038/s42254-022-00491-0)
- [24] Realizing exceptional points of any order in the presence of symmetry Sharareh Sayyad and Flore K. Kunst Phys. Rev. Research 4, 023130
- [25] PHYSICAL REVIEW RESEARCH 6, 023205 (2024)
- [26] Hassan, A. U., Hodaie, H., Miri, M.-A., Khajavikhan, M., and Christodoulides, D. N. "Nonlinear reversal of the

- PT-symmetric phase transition in a system of coupled semiconductor microring resonators." *Physical Review A* 92.6 (2015): 063807. DOI: [10.1103/PhysRevA.92.063807](https://doi.org/10.1103/PhysRevA.92.063807)
- [27] Liu, Y., and Zhang, X. "Recent advances in transformation optics." *Nanoscale* 4.17 (2012): 5277-5292. DOI: [10.1039/C2NR31140A](https://doi.org/10.1039/C2NR31140A)
- [28] Chen, H., Chan, C. T., and Sheng, P. "Transformation optics and metamaterials." *Nature Materials* 9.5 (2010): 387-396. DOI: [10.1038/nmat2743](https://doi.org/10.1038/nmat2743)
- [29] Makris, K. G., El-Ganainy, R., Christodoulides, D. N., and Musslimani, Z. H. "Beam dynamics in PT symmetric optical lattices." *Physical Review Letters* 100.10 (2008): 103904. DOI: [10.1103/PhysRevLett.100.103904](https://doi.org/10.1103/PhysRevLett.100.103904)
- [30] McCall, M., Pendry, J. B., Galdi, V., et al. "Roadmap on transformation optics." *Journal of Optics* 20.6 (2018): 063001. DOI: [10.1088/2040-8986/aac269](https://doi.org/10.1088/2040-8986/aac269)
- [31] Sun, F., Zheng, B., Chen, H., et al. "Transformation optics: From classic theory and applications to its new branches." *Laser & Photonics Reviews* 11.6 (2017): 1700034. DOI: [10.1002/lpor.201700034](https://doi.org/10.1002/lpor.201700034)
- [32] Kundtz, N. B., Smith, D. R., and Pendry, J. B. "Electromagnetic design with transformation optics." *Proceedings of the IEEE* 99.10 (2010): 1622-1633. DOI: [10.1109/JPROC.2011.2104310](https://doi.org/10.1109/JPROC.2011.2104310)
- [33] Pendry, J. B., Schurig, D., and Smith, D. R. "Controlling electromagnetic fields." *Science* 312.5781 (2006): 1780-1782. DOI: [10.1126/science.1125907](https://doi.org/10.1126/science.1125907)
- [34] S. Neumark, *Solution of Cubic and Quartic Equations* (Elsevier, 2014).
- [35] Aubry, A., Lei, D. Y., Maier, S. A., and Pendry, J. B. "Plasmonic hybridization between nanowires and a metallic surface: a transformation optics approach." *ACS Nano* 5.4 (2011): 3293-3308. DOI: [10.1021/nn200208a](https://doi.org/10.1021/nn200208a)
- [36] Pendry, J. B., Fernández-Domínguez, A. I., Luo, Y., and Zhao, R. "Capturing photons with transformation optics." *Nature Physics* 9.8 (2013): 518-522. DOI: [10.1038/nphys2667](https://doi.org/10.1038/nphys2667)
- [37] Yang, Honghua U., et al. "Optical dielectric function of silver." *Physical Review B* 91.23 (2015): 235137. DOI: [10.1103/PhysRevB.91.235137](https://doi.org/10.1103/PhysRevB.91.235137)
- [38] Garcia de Abajo, F. J. Nonlocal effects in the plasmons of strongly interacting nanoparticles, dimers, and waveguides. *J. Phys. Chem. C* 112, 17983–17987 (2008)
- [39] Savage, K. J. et al. Revealing the quantum regime in tunnelling plasmonics. *Nature* 491, 574–577 (2012).
- [40] Aubry, A., Lei, D. Y., Maier, S. A., et al. "Conformal transformation applied to plasmonics beyond the quasistatic limit." *Physical Review B—Condensed Matter and Materials Physics* 82.20 (2010): 205109. DOI: [10.1103/PhysRevB.82.205109](https://doi.org/10.1103/PhysRevB.82.205109)
- [41] Wang, K., Xiao, L., Lin, H., et al. "Experimental simulation of symmetry-protected higher-order exceptional points with single photons." *Science Advances* 9.34 (2023): eadi0732. DOI: [10.1126/sciadv.adi0732](https://doi.org/10.1126/sciadv.adi0732)
- [42] Chen, H. Z., Liu, T., Luan, H. Y., et al. "Revealing the missing dimension at an exceptional point." *Nature Physics* 16.5 (2020): 571-578. DOI: [10.1038/s41567-020-0824-y](https://doi.org/10.1038/s41567-020-0824-y)
- [43] Y. Gao, N. Zhou, Z. Shi, X. Guo, and L. Tong, "Dark dimer mode excitation and strong coupling with a nanorod dipole," *Photon. Res.* 6, 887 (2018).
- [44] D. E. Gómez, Z. Q. Teo, M. Altissimo, T. J. Davis, S. Earl, and A. Roberts, "The Dark Side of Plasmonics," *Nano Lett.* 13, 3722–3728 (2013).

Supplementary Information: Topological Engineering of High-Order Exceptional Points through Transformation Optics

Kaiyuan Wang ^{1,2} Qi Jie Wang ^{1,3} Matthew R. Foreman ^{1,2,*} and Yu Luo ^{4,†}

¹*School of Electrical and Electronic Engineering,
Nanyang Technological University, 50 Nanyang Avenue, Singapore 639798*

²*Institute for Digital Molecular Analytics and Science, 59 Nanyang Drive, Singapore 636921*

³*Centre for Disruptive Photonic Technologies, School of Physical and Mathematical Sciences,
Nanyang Technological University, Singapore, Singapore*

⁴*National Key Laboratory of Microwave Photonics,
Nanjing University of Aeronautics and Astronautics, Nanjing 211106, China*

(Dated: March 18, 2025)

S-I. INTRODUCTION

In our article we discuss the use of transformation optics for design of high order exceptional points in two-dimensional (2D) nanophotonic systems. Here we provide further mathematical details of our approach. In Section S-II we first derive the standard resonance condition for surface plasmon polariton (SPP) modes in a planar slab-like geometry. An alternative derivation is presented in Section S-III and extended to higher order geometries. Section S-IV A details how this result can be in turn used to identify second order exceptional points in an asymmetric core-shell nanowire structure. Sections S-IV B and S-IV C apply similar principles to study third and fourth order exceptional points in a coupled core-shell/monomer nanowire system and core-shell dimer system respectively.

S-II. THREE LAYER RESONANCE CONDITION

We consider the geometry shown in Figure S1(a) comprising of three regions of relative electric permittivity ϵ_1 , ϵ_2 and ϵ_3 respectively, separated by interfaces at $x = x_0$ and $x = x_0 + d$, and illuminated by a periodic array of electric line dipoles each with moment Δ . The line dipoles are assumed to lie in the left-most medium and located at $\mathbf{r}_m = (x_m, y_m) = (0, 2m\pi)$ for $m \in \mathbb{Z}$. Our choice of illumination is for later convenience when performing calculations in the transformed coordinate system, however, this choice does not affect the resonance condition.

We will assume that the quasi-static approximation holds, such that the electric potential $\phi(\mathbf{r})$ induced in the systems from the line dipoles satisfies Laplace's equation

$$\nabla^2 \phi(\mathbf{r}) = -\frac{1}{2\pi\epsilon_0} \sum_{m=-\infty}^{m=+\infty} \frac{\Delta \cdot (\mathbf{r} - \mathbf{r}_m)}{|\mathbf{r} - \mathbf{r}_m|^2} = \phi_0(\mathbf{r}), \quad (\text{S1})$$

where $\mathbf{r} = (x, y)$ is the 2D position vector and $\phi_0(\mathbf{r})$ is the source potential. The problem of determining the induced potential is easily solved in the Fourier domain [1, 2]. In an arbitrary plane x the source potential can be written in the form:

$$\phi_0(\mathbf{r}) = \frac{1}{2\pi} \int_{-\infty}^{\infty} \Phi_0(k, x) e^{iky} dk \quad (\text{S2})$$

* matthew.foreman@ntu.edu.sg

† yu.luo@nuaa.edu.cn

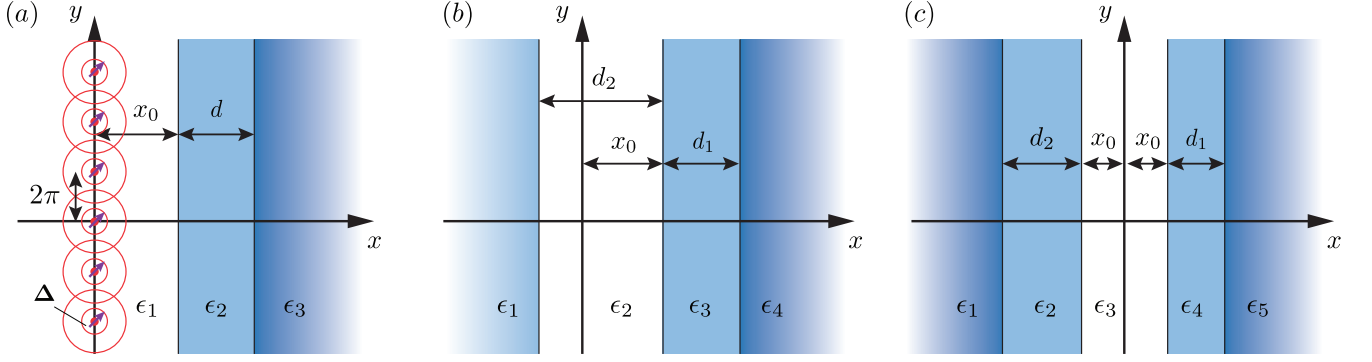


FIG. S1. Schematics of 2D planar multilayer geometries considered comprising of (a) 3, (b) 4 and (c) 5 distinct material regions.

where

$$\Phi_0(k, x) = -\frac{1}{2\pi\epsilon_0} \sum_{m=-\infty}^{m=+\infty} \int_{-\infty}^{\infty} \frac{\Delta \cdot (\mathbf{r} - \mathbf{r}_m)}{|\mathbf{r} - \mathbf{r}_m|^2} e^{-iky} dy \quad (\text{S3})$$

$$= -\frac{1}{2\pi\epsilon_0} \sum_{m=-\infty}^{m=+\infty} e^{-iky_m} \int \frac{\Delta \cdot \mathbf{r}}{|\mathbf{r}|^2} e^{-iky} dy \quad (\text{S4})$$

$$= \begin{cases} \mathcal{A}_+(k) e^{-|k|x} & \text{if } x > 0 \\ \mathcal{A}_-(k) e^{|k|x} & \text{if } x < 0 \end{cases} \quad (\text{S5})$$

where

$$\mathcal{A}_{\pm}(k) = -\frac{1}{2\epsilon_0} \sum_{m=-\infty}^{m=+\infty} e^{-iky_m} (\pm\Delta_x + i \text{sign}[k]\Delta_y) \quad (\text{S6})$$

$$= -\frac{1}{2\epsilon_0} \sum_{n=-\infty}^{n=+\infty} (\pm\Delta_x + i \text{sign}[k]\Delta_y) \delta(k - n) \quad (\text{S7})$$

and $\delta[k]$ denotes the Dirac delta function. From Equations (S5) and (S7), we note that the Fourier spectrum of the source potential is a Dirac comb. Accordingly, only modes associated with integer spatial frequencies n can be excited by the chosen source distribution.

Each Fourier component of the source potential $\Phi_0(k)$ induces a potential across all space which can be expressed in the form

$$\Phi(k, x) = \begin{cases} \mathcal{B}(k) e^{iky+|k|x} & \text{for } x \leq x_0 \\ \mathcal{C}(k) e^{iky-|k|x} + \mathcal{D}(k) e^{iky+|k|x} & \text{for } x_0 \leq x \leq x_0 + d \\ \mathcal{E}(k) e^{iky-|k|x} & \text{for } x_0 + d \leq x \end{cases} \quad (\text{S8})$$

where as a consequence of the Dirac delta functions in Equation (S7) $k = n$ ($n \in \mathbb{Z}$). Note the total potential in the Fourier domain is then $\Phi_0(k, x) + \Phi(k, x)$.

To find the resonance condition of the sheet geometry, we follow the standard procedure and enforce continuity of the tangential (normal) components of the electric (displacement) field \mathbf{E} (\mathbf{D}). Noting then that $\mathbf{E}(\mathbf{r}) = -\nabla\phi(\mathbf{r})$ and $\mathbf{D}(\mathbf{r}) = \epsilon\mathbf{E}(\mathbf{r})$ respectively, for a single Fourier component we have at $x = x_0$ (assuming $x_0 > 0$)

$$\mathcal{A}_+(k) e^{-|k|x_0} + \mathcal{B}(k) e^{|k|x_0} = \mathcal{C}(k) e^{-|k|x_0} + \mathcal{D}(k) e^{|k|x_0} \quad (\text{S9})$$

$$\epsilon_1 [\mathcal{A}_+(k) e^{-|k|x_0} - \mathcal{B}(k) e^{|k|x_0}] = \epsilon_2 [\mathcal{C}(k) e^{-|k|x_0} - \mathcal{D}(k) e^{|k|x_0}]. \quad (\text{S10})$$

Similarly at $x = x_0 + d$ it follows that

$$\mathcal{C}(k) e^{-|k|(x_0+d)} + \mathcal{D}(k) e^{|k|(x_0+d)} = \mathcal{E}(k) e^{-|k|(x_0+d)} \quad (\text{S11})$$

$$\epsilon_2 [\mathcal{C}(k) e^{-|k|(x_0+d)} - \mathcal{D}(k) e^{|k|(x_0+d)}] = \epsilon_3 \mathcal{E}(k) e^{-|k|(x_0+d)}. \quad (\text{S12})$$

Solving Equations (S9)–(S12) for the unknown amplitudes $\mathcal{B}(k)$, $\mathcal{C}(k)$, $\mathcal{D}(k)$ and $\mathcal{E}(k)$, yields

$$\mathcal{B}(k) = \left[\frac{\epsilon_2 - \epsilon_3}{\epsilon_2 + \epsilon_3} + \frac{\epsilon_1 - \epsilon_2}{\epsilon_1 + \epsilon_2} e^{2|k|d} \right] \frac{e^{-2|k|x_0}}{e^{2|k|d} - e^\beta} \mathcal{A}_+(k) \quad (\text{S13})$$

$$\mathcal{C}(k) = \frac{2\epsilon_1}{\epsilon_1 + \epsilon_2} \frac{e^{2|k|d}}{e^{2|k|d} - e^\beta} \mathcal{A}_+(k) \quad (\text{S14})$$

$$\mathcal{D}(k) = \frac{2\epsilon_1(\epsilon_2 - \epsilon_3)}{(\epsilon_1 + \epsilon_2)(\epsilon_2 + \epsilon_3)} \frac{e^{-2|k|x_0}}{e^{2|k|d} - e^\beta} \mathcal{A}_+(k) \quad (\text{S15})$$

$$\mathcal{E}(k) = \frac{4\epsilon_1\epsilon_2}{(\epsilon_1 + \epsilon_2)(\epsilon_2 + \epsilon_3)} \frac{e^{2|k|d}}{e^{2|k|d} - e^\beta} \mathcal{A}_+(k) \quad (\text{S16})$$

where

$$e^\beta = \frac{(\epsilon_2 - \epsilon_1)(\epsilon_2 - \epsilon_3)}{(\epsilon_1 + \epsilon_2)(\epsilon_2 + \epsilon_3)}. \quad (\text{S17})$$

Finally, we note from Equations (S13)–(S16) that the induced potential scales with $[\exp(2|k|d) - \exp(\beta)]^{-1}$ regardless of source potential. Resonances in the system are thus seen to occur when

$$e^{2|k|d} = \frac{(\epsilon_2 - \epsilon_1)(\epsilon_2 - \epsilon_3)}{(\epsilon_1 + \epsilon_2)(\epsilon_2 + \epsilon_3)}. \quad (\text{S18})$$

S-III. ALTERNATIVE DERIVATION

In this section we again seek to determine the resonance condition, however, present an alternative derivation which enables us to calculate the corresponding mode potentials more easily. This approach furthermore enables easy extension to the higher order geometries shown in Figure S1(b) and (c). We begin by considering the second order case (Figure S1(a)), in which we seek bound surface modes whose potential distribution takes the form of Equation (S8). We may express the tangential electric field components at $x = d_0$ and $x = d_0 + d$, denoted $E_{y,1}$ and $E_{y,2}$ respectively as

$$E_{y,1} = ik \mathcal{B}(k) e^{|k|x_0} \quad (\text{S19})$$

$$E_{y,1} = ik \left[\mathcal{C}(k) e^{-|k|x_0} + \mathcal{D}(k) e^{|k|x_0} \right] \quad (\text{S20})$$

$$E_{y,2} = ik \left[\mathcal{C}(k) e^{-|k|(x_0+d)} + \mathcal{D}(k) e^{|k|(x_0+d)} \right] \quad (\text{S21})$$

$$E_{y,2} = ik \mathcal{E}(k) e^{-|k|(x_0+d)}. \quad (\text{S22})$$

The normal components of the displacement, $D_{x,1}$ and $D_{x,2}$, can similarly be expressed

$$D_{x,1} = \epsilon_1 |k| \mathcal{B}(k) e^{|k|x_0} \quad (\text{S23})$$

$$D_{x,1} = \epsilon_2 |k| \left[-\mathcal{C}(k) e^{-|k|x_0} + \mathcal{D}(k) e^{|k|x_0} \right] \quad (\text{S24})$$

$$D_{x,2} = \epsilon_2 |k| \left[-\mathcal{C}(k) e^{-|k|(x_0+d)} + \mathcal{D}(k) e^{|k|(x_0+d)} \right] \quad (\text{S25})$$

$$D_{x,2} = -\epsilon_3 |k| \mathcal{E}(k) e^{-|k|(x_0+d)}. \quad (\text{S26})$$

Eliminating $\mathcal{B}(k)$, $\mathcal{C}(k)$, $\mathcal{D}(k)$, $\mathcal{E}(k)$, $D_{x,1}$ and $D_{x,2}$ from Equations (S19)–(S26) yields two linear equations for $E_{y,1}$ and $E_{y,2}$, which written in matrix form reads

$$\begin{bmatrix} 1 + (\epsilon_2/\epsilon_1)\tanh(|k|d) & (\epsilon_3/\epsilon_1)\text{sech}(|k|d) \\ -\text{sech}(|k|d) & 1 + (\epsilon_3/\epsilon_2)\tanh(|k|d) \end{bmatrix} \begin{bmatrix} E_{y,1} \\ E_{y,2} \end{bmatrix} \triangleq \mathbb{M}^{(2)} \mathbf{E}^{(2)} = \mathbf{0}_2 \quad (\text{S27})$$

where $\mathbf{0}_p$ is a $p \times 1$ vector of zeros. Equation (S27) only has non-trivial solutions when the matrix \mathbb{M} has zero determinant, i.e. $\det[\mathbb{M}^{(2)}] = 0$, or equivalently

$$(\epsilon_2^2 + \epsilon_1\epsilon_3)\tanh(|k|d) + \epsilon_2(\epsilon_1 + \epsilon_3) = 0. \quad (\text{S28})$$

It is easy to show that Equation (S28) is equivalent to Equation (S18). The advantage of expressing the resonance condition in the form of Equation (S27) is that we can also determine the form of the potential and field distributions on resonance. Specifically, through Gaussian elimination it can be shown that the solution to Eq. (S27) when Eq. (S28) holds, is given by

$$\mathbf{E}^{(2)} = \begin{bmatrix} 1 \\ -\epsilon_3^{-1}[\epsilon_1 \sinh(|k|d) + \epsilon_2 \cosh(|k|d)] \end{bmatrix}. \quad (\text{S29})$$

Extension of the derivations given above to the three and four interface cases shown in Figure S1(b) and (c) follows analogous steps. We find for the three interface case that

$$\mathbb{M}^{(3)} \mathbf{E}^{(3)} = \begin{bmatrix} \mathcal{M}(d_2, \epsilon_2, \epsilon_1) & -\epsilon_2 & 0 \\ 0 & -\epsilon_3 & \mathcal{M}(d_1, \epsilon_3, \epsilon_4) \\ \mathcal{M}(d_2, \epsilon_1, \epsilon_2) & 0 & \mathcal{M}(d_1, \epsilon_4, \epsilon_3) \end{bmatrix} \begin{bmatrix} E_y(x_0 - d_2) \\ E_y(x_0) \\ E_y(x_0 + d_1) \end{bmatrix} = \mathbf{0}_3 \quad (\text{S30})$$

where, omitting the k dependence for clarity,

$$\mathcal{M}(d, \epsilon_a, \epsilon_b) = \epsilon_a \cosh(|k|d) + \epsilon_b \sinh(|k|d) \quad (\text{S31})$$

such that the resonance condition can be expressed as

$$\det[\mathbb{M}^{(3)}] = \epsilon_2 \mathcal{M}(d_1, \epsilon_3, \epsilon_4) \mathcal{M}(d_2, \epsilon_1, \epsilon_2) + \epsilon_3 \mathcal{M}(d_1, \epsilon_4, \epsilon_3) \mathcal{M}(d_2, \epsilon_2, \epsilon_2) = 0. \quad (\text{S32})$$

On resonance, the solutions to Equation (S30) are of the form

$$\mathbf{E}^{(3)} = \begin{bmatrix} E_y(x_0 - d_2) \\ E_y(x_0) \\ E_y(x_0 + d_1) \end{bmatrix} = \begin{bmatrix} 1 \\ \epsilon_2^{-1} \mathcal{M}(d_2, \epsilon_2, \epsilon_1) \\ \epsilon_3 \mathcal{M}(d_2, \epsilon_2, \epsilon_1) / [\epsilon_2 \mathcal{M}(d_2, \epsilon_3, \epsilon_4)] \end{bmatrix}. \quad (\text{S33})$$

For the four interface geometry of Figure S1(c) we have $\mathbb{M}^{(4)} \mathbf{E}^{(4)} = \mathbf{0}_4$ where

$$\mathbb{M}^{(4)} = \begin{bmatrix} \mathcal{M}(d_2, \epsilon_2, \epsilon_1) & -\epsilon_2 & 0 & 0 \\ \coth(2|k|x_0) \mathcal{M}(d_2, \epsilon_1, \epsilon_2) & \epsilon_3 & 0 & \text{cosech}(2|k|x_0) \mathcal{M}(d_1, \epsilon_5, \epsilon_4) \\ \text{cosech}(2|k|x_0) \mathcal{M}(d_2, \epsilon_1, \epsilon_2) & 0 & \epsilon_3 & \coth(2|k|x_0) \mathcal{M}(d_1, \epsilon_5, \epsilon_4) \\ 0 & 0 & -\epsilon_4 & \mathcal{M}(d_1, \epsilon_4, \epsilon_5) \end{bmatrix} \quad (\text{S34})$$

with resonance condition

$$\begin{aligned} & \epsilon_3 \mathcal{M}(d_1, \epsilon_4, \epsilon_5) [\epsilon_2 \coth(2|k|x_0) \mathcal{M}(d_2, \epsilon_1, \epsilon_2) + \epsilon_3 \mathcal{M}(d_2, \epsilon_2, \epsilon_1)] \\ & + \epsilon_4 \mathcal{M}(d_1, \epsilon_5, \epsilon_4) [\epsilon_2 \mathcal{M}(d_2, \epsilon_1, \epsilon_2) + \epsilon_3 \coth(2|k|x_0) \mathcal{M}(d_2, \epsilon_2, \epsilon_1)] = 0 \end{aligned} \quad (\text{S35})$$

and with corresponding solution, $\mathbf{E}^{(4)}$, of

$$\begin{bmatrix} E_y(-x_0 - d_2) \\ E_y(-x_0) \\ E_y(x_0) \\ E_y(x_0 + d_1) \end{bmatrix} = \begin{bmatrix} 1 \\ \epsilon_2^{-1} \mathcal{M}(d_2, \epsilon_2, \epsilon_1) \\ \epsilon_2^{-1} \cosh(2|k|x_0) \mathcal{M}(d_2, \epsilon_2, \epsilon_1) + \epsilon_3^{-1} \sinh(2|k|x_0) \mathcal{M}(d_2, \epsilon_1, \epsilon_2) \\ -[\epsilon_2 \cosh(2|k|x_0) \mathcal{M}(d_2, \epsilon_1, \epsilon_2) + \epsilon_3 \sinh(2|k|x_0) \mathcal{M}(d_2, \epsilon_2, \epsilon_1)] / [\epsilon_2 \mathcal{M}(d_1, \epsilon_5, \epsilon_4)] \end{bmatrix}. \quad (\text{S36})$$

S-IV. ENGINEERING EXCEPTIONAL POINTS IN NANOWIRE SYSTEMS

To study the properties of nanowire systems we can apply the principles of transformation optics to transform from the planar geometries of Figure S1, to those shown in Figure S2. Specifically, defining $w = x + iy$ in the original coordinates, and $w' = x' + iy'$ in the transformed coordinates we use the conformal transform

$$w' = \frac{g}{\exp(w) - 1} \quad (\text{S37})$$

where g is a constant that controls the size of the transformed cylinder(s). Specifically, the diameters of the cylinders for the core-shell nanowire of Figure S2(a) are

$$D_1 = \frac{g}{\exp(x_0 + d) - 1} + \frac{g}{\exp(x_0 + d) + 1} = g \text{cosech}(x_0 + d) \quad (\text{S38})$$

$$D_2 = \frac{g}{\exp(x_0) - 1} + \frac{g}{\exp(x_0) + 1} = g \text{cosech}(x_0) \quad (\text{S39})$$

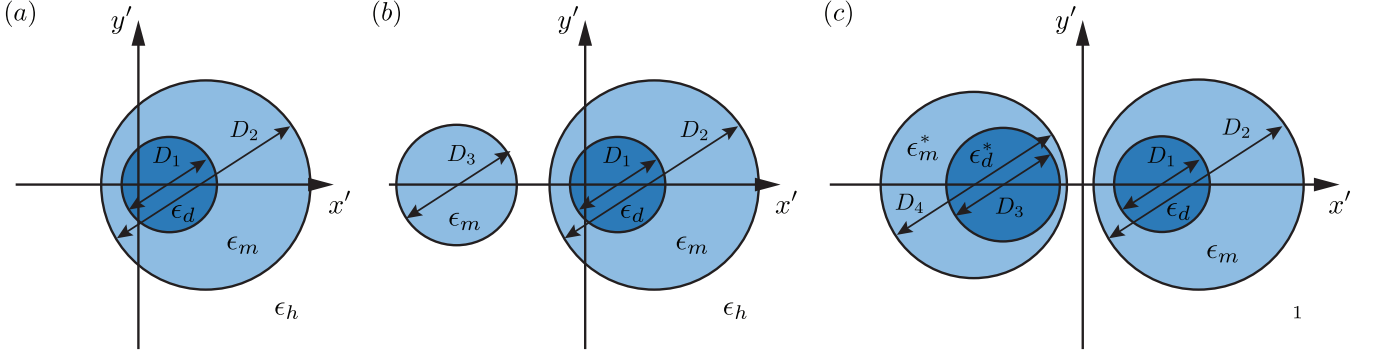


FIG. S2. Schematics of geometries from Figure S2 under the action of the conformal transform given by Eq. (S37), with material choices considered in Sections S-IV A-S-IV C

For the core-shell and monomer structure shown in Figure S2(b) we have $D_1 = g \operatorname{cosech}(x_0 + d_2)$, $D_2 = g \operatorname{cosech}(x_0)$ and $D_3 = g \operatorname{cosech}(x_0 - d_2)$, whilst for the core-shell dimer geometry of Figure S2(c) we have similarly $D_1 = g \operatorname{cosech}(x_0 + d_1)$, $D_2 = D_4 = g \operatorname{cosech}(x_0)$ and $D_3 = g \operatorname{cosech}(x_0 + d_2)$.

Under the conformal transform the electrostatic potential is preserved [3], i.e. $\phi(x, y) = \phi'(x', y')$ whilst the electric permittivity and magnetic permeability tensors transform according to $\bar{\epsilon}'_j = \epsilon_j \mathbb{J} \mathbb{J}^T / \det[\mathbb{J}]$ and $\bar{\mu}'_j = \mu_j \mathbb{J} \mathbb{J}^T / \det[\mathbb{J}]$, where we have assumed all media are isotropic in the origin system, and

$$\mathbb{J} = \frac{g}{2(\cosh x \cos y)^2} \begin{bmatrix} 1 - \cosh x \cos y & -\sinh x \sin y & 0 \\ \sinh x \sin y & 1 - \cosh x \cos y & 0 \\ 0 & 0 & 2g^{-1}(\cosh x - \cos y)^2 \end{bmatrix} \quad (\text{S40})$$

is the Jacobian matrix for the transform given in Equation (S37). Consequently the transformed tensors are of the form

$$\frac{\bar{\epsilon}'_j}{\epsilon_j} = \frac{\bar{\mu}'_j}{\mu_j} = \begin{bmatrix} 1 & 0 \\ 0 & 1 \\ 0 & 0 & 4(\cos y - \cosh x)^2/g^2 \end{bmatrix}. \quad (\text{S41})$$

In the quasi-static limit, in which the dimensions of the relevant regions of interest are smaller than the optical wavelength, we may neglect the retardation effects as described by the spatial dependence of these material tensors. Consequently, we see that the electric permittivity and magnetic permeability of each region are also preserved under the action of Equation (S37). Furthermore, we note that solution of the electrostatic problem (as described by Laplace's equation) restricts our discussion to transverse-magnetic (TM, or equivalently p -polarised) modes [4].

A. Core-shell nanowire (2nd order EP)

With the transformation complete, we now consider the asymmetric core-shell geometry shown in Figure S2(a). We consider a metallo-dielectric core-shell nanowire in a host material, such that $\epsilon_1 = \epsilon_h$, $\epsilon_2 = \epsilon_m$ and $\epsilon_3 = \epsilon_d$ whereby the resonance condition becomes

$$(\epsilon_m^2 + \epsilon_h \epsilon_d) \tanh(nd) + \epsilon_m(\epsilon_d + \epsilon_h) = 0. \quad (\text{S42})$$

Note that the periodicity in the transform implies $k = n$ ($n \in \mathbb{Z}$) in a similar fashion to that seen in Section S-II and that ϵ_d is in general complex accounting for gain or loss in the dielectric. Note also that generally, solutions to Equation (S-II) require $n \neq 0$. Expressing Equation (S42) as a quadratic equation in ϵ_m , i.e.,

$$\epsilon_m^2 \tanh(nd) + \epsilon_m(\epsilon_d + \epsilon_h) + \epsilon_h \epsilon_d \tanh nd = 0 \quad (\text{S43})$$

we can solve for values ϵ_m , or equivalently (by virtue of the material dispersion) optical frequencies, at which resonances occur. The resonant modes however become degenerate when Equation (S43) has a repeated root, i.e. when

$$(\epsilon_h + \epsilon_d)^2 = 4\epsilon_h \epsilon_d \tanh^2(nd). \quad (\text{S44})$$

or equivalently

$$\epsilon_d = \epsilon_h [2 \tanh^2(nd) - 1 \pm 2i \tanh(nd) \operatorname{sech}(nd)]. \quad (\text{S45})$$

Substituting Equation (S44) into Equation (S43) and solving subsequently yields

$$\epsilon_m = -\frac{\epsilon_h + \epsilon_d}{2} \coth nd = -\epsilon_h [\tanh(nd) \mp i \operatorname{sech}(nd)]. \quad (\text{S46})$$

B. Coupled core-shell/monomer nanowires (3rd order EP)

We now consider the coupled nanowire structures depicted in Figure S2(b) where we assume $\epsilon_1 = \epsilon_m$, $\epsilon_2 = 1$, $\epsilon_3 = \epsilon_m$ and $\epsilon_4 = \epsilon_d$. Note that the two wire system depicted requires $d_2 > x_0$, otherwise a single three-layer nanowire structure results which is not our case of interest. With these replacements Equation (S32) can be written as a cubic equation in ϵ_m

$$A\epsilon_m^3 + B\epsilon_m^2 + C\epsilon_m + D = 0 \quad (\text{S47})$$

where

$$A = \sinh(nd_1) \sinh(nd_2) \quad (\text{S48})$$

$$B = \epsilon_h \cosh(nd_1) \cosh(nd_2) + \epsilon_h \sinh(nd_1) \cosh(nd_2) + \epsilon_d \cosh(nd_1) \sinh(nd_2) \quad (\text{S49})$$

$$C = \epsilon_h \epsilon_d \cosh(nd_1) \cosh(nd_2) + \epsilon_h \epsilon_d \sinh(nd_1) \cosh(nd_2) + \epsilon_h^2 \cosh(nd_1) \sinh(nd_2) \quad (\text{S50})$$

$$D = \epsilon_d \epsilon_h^2 \sinh(nd_1) \sinh(nd_2) \quad (\text{S51})$$

and $n \neq 0$. The roots of Equation (S47) are all identical if

$$3AC - B^2 = 0 \quad (\text{S52})$$

$$27A^2D - 9ABC + 2B^3 = 0 \quad (\text{S53})$$

and take the form

$$\epsilon_m = -\frac{B}{3A} = \frac{1}{3} [\epsilon_h [1 + \coth(nd_1)] \coth(nd_2) + \epsilon_d \coth(nd_1)] \quad (\text{S54})$$

as discussed in the main text.

C. Coupled core-shell/core-shell nanowires (4th order EP)

Finally, we consider the core-shell dimer type structure shown in Figure S2(c). We assume a parity time symmetric configuration whereby $d_1 = d_2 = d$, $\epsilon_1 = \epsilon_d^*$, $\epsilon_2 = \epsilon_m^*$, $\epsilon_3 = 1$, $\epsilon_4 = \epsilon_m$ and $\epsilon_5 = \epsilon_d$. We further assume $\epsilon_m = \epsilon_\infty - \omega_p^2/\omega^2 + i\alpha$, whereas $\epsilon_d = \epsilon - i\beta$. Substituting these parameters into Equation (S35) yields the polynomial express

$$A\omega^8 + B\omega^6 + C\omega^4 + D\omega^2 + E = 0 \quad (\text{S55})$$

where

$$\begin{aligned}
A = \frac{1}{8} \operatorname{cosech}(nx_0) \operatorname{sech}(nx_0) & \left[(\alpha^2 + (\epsilon_\infty - 1)^2) (\alpha^2 + \beta^2 + \epsilon^2 + \epsilon_\infty^2) \sinh[2n(x_0 - d)] \right. \\
& + 2(\alpha^2 + (\epsilon_\infty - 1)^2) (\alpha\beta - \epsilon\epsilon_\infty) \cosh[2n(x_0 - d)] \\
& - 2(\alpha^2 + \epsilon_\infty^2 - 1) (\alpha^2 - \beta^2 - \epsilon^2 + \epsilon_\infty^2) \sinh[2nx_0] \\
& + 8\alpha(\alpha\epsilon + \beta\epsilon_\infty) \cosh[2nx_0] \\
& + (\alpha^2 + (\epsilon_\infty + 1)^2) (\alpha^2 + \beta^2 + \epsilon^2 + \epsilon_\infty^2) \sinh[2n(x_0 + d)] \\
& \left. + 2(\alpha^2 + (\epsilon_\infty + 1)^2) (\alpha\beta - \epsilon\epsilon_\infty) \cosh[2n(x_0 + d)] \right] \quad (\text{S56})
\end{aligned}$$

$$\begin{aligned}
B = \frac{1}{4} \omega_p^2 \operatorname{cosech}(nx_0) \operatorname{sech}(nx_0) & \left[(\alpha^2(1 - 2\epsilon_\infty) - (\epsilon_\infty - 1)(\beta^2 + \epsilon^2 + \epsilon_\infty(2\epsilon_\infty - 1))) \sinh[2n(x_0 - d)] \right. \\
& + (\alpha^2\epsilon - 2\alpha\beta(\epsilon_\infty - 1) + \epsilon\epsilon_\infty(3\epsilon_\infty - 4) + \epsilon) \cosh[2n(x_0 - d)] \\
& + 2\epsilon_\infty(2\alpha^2 - \beta^2 - \epsilon^2 + 2\epsilon_\infty^2 - 1) \sinh[2nx_0] - 4\alpha\beta \cosh[2nx_0] \\
& + (-\alpha^2(2\epsilon_\infty + 1) - (\epsilon_\infty + 1)(\beta^2 + \epsilon^2 + 2\epsilon_\infty^2 + \epsilon_\infty)) \sinh[2n(x_0 + d)] \\
& \left. + (\alpha^2\epsilon - 2\alpha\beta(\epsilon_\infty + 1) + \epsilon(\epsilon_\infty + 1)(3\epsilon_\infty + 1)) \cosh[2n(x_0 + d)] \right] \quad (\text{S57})
\end{aligned}$$

$$\begin{aligned}
C = \frac{1}{4} \omega_p^4 \operatorname{cosech}(2nx_0) & \left[(1 + 2\alpha^2 + \beta^2 + \epsilon^2 - 6\epsilon_\infty(\epsilon_\infty - 1)) \sinh[2n(x_0 - d)] \right. \\
& + (\epsilon(4 - 6\epsilon_\infty) + 2\alpha\beta) \cosh[2n(x_0 - d)] \\
& + (1 + 2\alpha^2 + \beta^2 + \epsilon^2 + 6\epsilon_\infty(\epsilon_\infty + 1)) \sinh[2n(x_0 + d)] \\
& + (-2\alpha\beta + 6\epsilon\epsilon_\infty + 4\epsilon) \cosh[2n(x_0 + d)] \\
& \left. + (1 - 2\alpha^2 + \beta^2 + \epsilon^2 - 6\epsilon_\infty^2) 2 \sinh[2nx_0] \right] \quad (\text{S58})
\end{aligned}$$

$$D = -\omega_p^6 \left[4\epsilon_\infty \sinh[nd] \coth[nx_0] + \cosh[nd] (2\epsilon \coth[nx_0] + \coth^2[nx_0] + 1) \right] \sinh[nd] \tanh[nx_0] \quad (\text{S59})$$

$$E = \omega_p^8 \sinh^2(nd) \quad (\text{S60})$$

Equation (S55) is a quartic equation in ω^2 , the solutions to which are identical if

$$8AC - 3B^2 = 0 \quad (\text{S61})$$

$$B^3 - 4ABC + 8A^2D = 16AB^2C - 64A^2BD - 3B^4 + 256A^3E = 0 \quad (\text{S62})$$

Denoting these solutions as $\Xi = \omega_r^2 = -B/4A$, we can then find the eigenfrequencies $\omega_r = \pm\sqrt{\Xi}$, where solutions for which the real part is negative are discarded.

-
- [1] D. Y. Lei, A. Aubry, S. A. Maier, and J. B. Pendry, "Broadband nano-focusing of light using kissing nanowires," *New J. Phys.* 12, 093030 (2010).
[2] A. Aubry, D. Y. Lei, S. A. Maier, and J. B. Pendry, "Plasmonic Hybridization between Nanowires and a Metallic Surface: A Transformation Optics Approach," *ACS Nano* 5, 3293–3308 (2011).
[3] J. Zhang, J. B. Pendry, and Y. Luo, "Transformation optics from macroscopic to nanoscale regimes: a review," *Adv. Photon.* 1, 014001 (2019).
[4] J. B. Pendry, "Negative Refraction Makes a Perfect Lens," *Phys. Rev. Lett.* 85, 3966–3969 (2000).